Eur. Phys. J. E (2021) 44:78
https://doi.org/10.1140/epje/s10189-021-00085-y

THE EUROPEAN PHYSICAL JOURNAL E

Regular Article – Soft Matter

Parametric excitation of wrinkles in elastic sheets on elastic and viscoelastic substrates

Haim Diamant[a]

School of Chemistry, Center for Physics and Chemistry of Living Systems, Tel Aviv University, Tel Aviv 6997801, Israel

Received 9 February 2021 / Accepted 1 June 2021 / Published online 14 June 2021

Abstract Thin elastic sheets supported on compliant media form wrinkles under lateral compression. Since the lateral pressure is coupled to the sheet's deformation, varying it periodically in time creates a parametric excitation. We study the resulting parametric resonance of wrinkling modes in sheets supported on semi-infinite elastic or viscoelastic media, at pressures smaller than the critical pressure of static wrinkling. We find distinctive behaviors as a function of excitation amplitude and frequency, including (a) a different dependence of the dynamic wrinkle wavelength on sheet thickness compared to the static wavelength; and (b) a discontinuous decrease in the dominant wrinkle wavelength upon increasing excitation frequency at sufficiently large pressures. In the case of a viscoelastic substrate, resonant wrinkling requires crossing a threshold of excitation amplitude. The frequencies for observing these phenomena in relevant experimental systems are of the order of a kilohertz and above. We discuss experimental implications of the results.

1 Introduction

Wrinkling is one of the common deformation patterns which thin elastic sheets form when subjected to lateral compression [1–3]. In many cases, wrinkles appear when the sheet is supported on a softer substrate, a scenario which is relevant to a range of applications (e.g., coatings, paints) and naturally occurring structures (e.g., skin and tissue linings). Studies have been directed more recently at *active* wrinkling [4–8]. The interplay between the topography of supported thin sheets and their delamination off the support [9–13] suggests active wrinkling as an anti-fouling strategy adopted by Nature and mimicked in man-made systems [5,6,8,14]. These studies of active wrinkling have considered static or quasi-static wrinkles, arising from mechanical equilibrium at pressures exceeding the static flat-to-wrinkle transition. The dynamic effects considered in those studies [5,8] are due to low-frequency (below 1 Hz) actuations, where the wrinkles follow the external stimulus quasi-statically.

Works going beyond the quasi-static limit addressed the time evolution of the flat-to-wrinkle transition in sheets supported on viscous [15,16] and viscoelastic [17] media. Dynamic wrinkles have been studied in two additional scenarios. The first is the formation of radial wrinkles in thin sheets upon impact of a rigid object [18–21]. In another scenario, a slender body in contact with a liquid is compressed by a progressively increasing lateral pressure [22–24]. Unlike static wrinkles, whose wavelength is determined by a competition between two restoring forces (e.g., bending of the sheet and deformation of the substrate), those short-time dynamic wrinkles arise from an interplay of a restoring force and inertia or viscous stresses in the substrate, resulting in a wavelength that increases with time. Finally, dynamic control of wrinkle wavelength and pattern was demonstrated in supported sheets under changing temperature and solvent diffusion [25].

The present work investigates a different phenomenon, where periodic forcing and inertia take a supported sheet out of plane through a mechanism of parametric resonance [26]. Parametric resonance suggests itself naturally for compressed sheets, because the actuating pressure produces a force that depends on the sheet's out-of-plane deformation.

The investigated dynamics involves a combination of five factors: the sheet's bending elasticity and inertia, and the substrate's elasticity, viscosity, and inertia. Section 2 is devoted, therefore, to heuristic consideration of the relevant scales and dominant mechanisms. In addition, to reduce the complexity of the analysis, we will employ along the way several simplifying assumptions while trying not to compromise the qualitative physical significance of the results. In Sect. 3, we present the model and the general equations of motion which are common to the more specific cases that follow. Section 4 presents results for a sheet supported on two types of substrate — an elastic substrate (Sect. 4.1) and a viscoelastic one (Sect. 4.2). We give in the main text the key steps of the derivations and their results. The detailed calculations are found in the Supplementary

[a] e-mail: hdiamant@tau.ac.il (corresponding author)

Material [27]. In Sect. 5, we summarize the predictions for experiments, compare the resonant wrinkling with other dynamic-wrinkling scenarios and describe potential extensions of the theory.

2 Relevant scales

Let us examine the relevant scales and dominant mechanisms of the suggested phenomenon. As mentioned above, five physical mechanisms are at play (a) the substrate's elasticity, characterized by a shear modulus G; (b) the sheet's rigidity, characterized by a bending modulus B; (c) the substrate's inertia, characterized by a three-dimensional (3D) mass density ρ_{m}; (d) the sheet's inertia, characterized by a 2D mass density $\rho = \rho_{\mathrm{s}} h$, where ρ_{s} is the sheet's 3D mass density and h its thickness; (e) in the case of a viscoelastic medium, the substrate's viscosity η.

Statically, the competition between the rigidities of the sheet and supporting medium gives rise to an intrinsic length which determines the wavelength of static wrinkles [1,2]. For a semi-infinite elastic substrate, the competition between (a) and (b) above gives the intrinsic length as $\lambda_{\mathrm{c}} \sim (B/G)^{1/3}$ [28]. In terms of the Young moduli of the sheet and medium, E_{s} and E_{m}, it can be rewritten as $\lambda_{\mathrm{c}} \sim h(E_{\mathrm{s}}/E_{\mathrm{m}})^{1/3}$. Thus, sheets that are orders of magnitude stiffer than the medium are required to obtain wrinkles with wavelength appreciably larger than h.

Dynamically, for a given length scale q^{-1}, the balance between one of the restoring forces and one of the inertial effects determines (by dimensional analysis) a characteristic frequency. Each of these balances gives the frequency–wavenumber relation for a limiting resonance mechanism. Balancing (a) and (c) above gives $\omega_{\mathrm{ac}} \sim (G/\rho_{\mathrm{m}})^{1/2} q$; this is the relation for Rayleigh waves on the surface of a sheet-free medium [29]. The combination of (b) and (c) gives $\omega_{\mathrm{bc}} \sim (B/\rho_{\mathrm{m}})^{1/2} q^{5/2}$. Taking (a) and (d), we find $\omega_{\mathrm{ad}} \sim (G/\rho)^{1/2} q^{1/2}$. Finally, (b) and (d) give $\omega_{\mathrm{bd}} \sim (B/\rho)^{1/2} q^2$; this is the relation for bending waves along a substrate-free sheet.

Assuming $h \ll q^{-1} \sim \lambda_{\mathrm{c}}$, one finds $\omega_{\mathrm{ac}} \sim \omega_{\mathrm{bc}} \ll \omega_{\mathrm{ad}} \sim \omega_{\mathrm{bd}}$. This implies that the dominant inertial effect usually comes from the substrate rather than the sheet. Hence, although the theory formulated below accounts for the inertia of both components, we will subsequently concentrate on the limit of substrate-dominated inertia. In this limit, we expect a crossover in the relation between actuation frequency and actuated wavenumber, around $q \sim \lambda_{\mathrm{c}}^{-1}$, from $\omega \sim \omega_{\mathrm{ac}} \sim q$ to $\omega \sim \omega_{\mathrm{bc}} \sim q^{5/2}$.[1]

Thus, the frequency $\omega_{\mathrm{m}} \sim (G/\rho_{\mathrm{m}})^{1/2}/\lambda_{\mathrm{c}}$, obtained from ω_{ac} or ω_{bc} for $q \sim \lambda_{\mathrm{c}}^{-1}$, sets the scale for the actuation frequency required to excite wrinkles of wavelength $\sim \lambda_{\mathrm{c}}$. For $G > 10^3$ Pa and $\lambda_{\mathrm{c}} < 1$ mm, we get $\omega_{\mathrm{m}} > 10^3$ Hz. Such frequencies probably lie outside the range of natural scenarios but are experimentally relevant.

In the case of a viscoelastic substrate, for the viscous damping to be appreciable, we need $\eta > G/\omega_{\mathrm{m}} \sim (G\rho_{\mathrm{m}})^{1/2}\lambda_{\mathrm{c}}$. With the bounds above, this gives $\eta > 1$ Pa s, i.e., more than 10^3 times the viscosity of water.

These conclusions are borne out by the detailed analysis that follows.

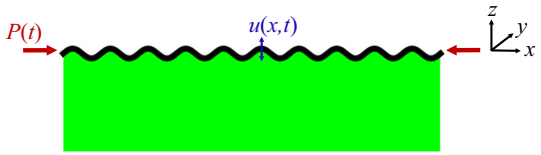

Fig. 1 Schematic view of the system

3 Model

3.1 The system

We consider a thin elastic sheet attached to the surface of a (visco)elastic medium. The sheet, lying at rest on the $z = 0$ plane, is assumed to be incompressible, infinite, and made of a much stiffer material than the supporting medium. The medium occupies the region $z \in (-\infty, 0)$. The sheet is compressed unidirectionally, along the x axis, by a time-dependent actuating pressure (force per unit length) $P(t)$. It can deform on the xz plane from $z = 0$ to $z = u(x,t)$. See Fig. 1. We assume $|\partial_x u| \ll 1$ and construct the leading-order (linear) model. Within this approximation, the extension from a one-dimensional surface deformation $u(x,t)$ to a two-dimensional one, $u(x,y,t)$, is simple, and we restrict the discussion to 1D for brevity.

3.2 Equations of motion

Both sheet and medium respond to the surface deformation $u(x,t)$. The sheet experiences a restoring normal force per unit area due to bending and the lateral compression,

$$F_{\mathrm{s}}(x,t) = -Bu'''' - P(t)u'', \tag{1}$$

where a prime denotes an x-derivative. We take the actuating pressure to be

$$P(t) = P_0 + P_1 \cos(\omega_1 t), \tag{2}$$

where P_0 is the static pressure, P_1 the actuation amplitude, and ω_1 the actuation frequency.

[1] The opposite limit, of sheet-dominated inertia, is analyzed in the Supplementary Material [27]. In this limit, we expect a crossover from $\omega \sim \omega_{\mathrm{bd}} \sim q^2$ to $\omega \sim \omega_{\mathrm{ad}} \sim q^{1/2}$

The normal force per unit area which the medium experiences at its surface is given by the general linear response,

$$F_{\rm m}(x,t) = \int_{-\infty}^{t} {\rm d}t' \int_{-\infty}^{\infty} {\rm d}x' K(x-x', t-t') u(x', t'). \tag{3}$$

The kernel $K(x,t)$ encodes the effect of the medium's spatial and temporal response on normal stresses at its surface. In Fourier space, $\tilde{K}(q,\omega) \equiv \int_{-\infty}^{\infty} {\rm d}t \int_{-\infty}^{\infty} {\rm d}x e^{iqx - i\omega t} K(x,t)$ is a complex function arising from the medium's viscoelasticity and inertia. We will assume a function of the form

$$\tilde{K}(q,\omega) \simeq K_0(q) + i\omega K_1(q) - \omega^2 K_2(q). \tag{4}$$

The first and third terms are motivated by the surface response of an elastic medium in *both limits* of low and high frequency (see below). These time-reversible responses relate to the elastic restoring force (first term), and the substrate's inertia (third term). The second, time-irreversible term corresponds to the viscous component of the response. We assume for simplicity that, within the relevant frequency range, the viscous coefficient K_1 does not change with frequency (i.e., the viscoelasticity is dominated by a single relaxation process with rate K_0/K_1). Note that Eq. (4) can be obtained by expanding $\tilde{K}$ in a small range of frequencies around any given frequency.

The equation of motion for the sheet's deformation is

$$\rho \ddot{u} = F_{\rm s} - F_{\rm m}, \tag{5}$$

where $\rho \equiv \rho_{\rm s} h$ is the sheet's mass per unit area, and a dot denotes a time derivative. Using Eqs. (1)–(5) while applying a spatial Fourier transform, $\tilde{f}(q,t) \equiv \int_{-\infty}^{\infty} {\rm d}x e^{iqx} f(x,t)$, turns the equation of motion into

$$[\rho + K_2(q)]\ddot{\tilde{u}} + K_1(q)\dot{\tilde{u}} + [Bq^4 - P(t)q^2 + K_0(q)]\tilde{u} = 0. \tag{6}$$

The transformation

$$\tilde{v} \equiv \tilde{u} e^{-[K_1/(2(\rho+K_2))]t} \tag{7}$$

eliminates the friction term, yielding

$$(\rho + K_2)\ddot{\tilde{v}} + [Bq^4 - P(t)q^2 + K_0 - K_1^2/(4(\rho+K_2))]\tilde{v} = 0. \tag{8}$$

We rewrite Eq. (8) as

$$\ddot{\tilde{v}} + \omega_0^2[1 + a\cos((2\omega_0 + \epsilon)t)]\tilde{v} = 0, \tag{9}$$

where

$$\begin{aligned} \omega_0^2(q) &\equiv \frac{1}{\rho + K_2}\left(Bq^4 - P_0 q^2 + K_0 - \frac{K_1^2}{4(\rho+K_2)}\right), \\ a(q) &\equiv -\frac{P_1 q^2}{\omega_0^2}, \\ \epsilon(q) &\equiv \omega_1 - 2\omega_0(q). \end{aligned} \tag{10}$$

The problem has been transformed into an analogous chain of independent, parametrically actuated oscillators, with intrinsic frequencies $\omega_0(q)$, actuation amplitudes $a(q)$, and detuning parameters $\epsilon(q)$. We see in Eq. (10) that increasing the static pressure P_0 weakens the 'spring constant' ω_0^2. For the analogy to work, we must have

$$\omega_0^2(q) > 0, \tag{11}$$

and 'oscillators' (modes) q which do not satisfy it are damped. Further, from the known solution to the classical problem of parametric resonance [26], we infer the condition for instability (i.e., exponentially growing amplitude $\tilde{u}(q,t)$), to leading order in the actuation a,

$$\Gamma^2(q) \equiv \frac{1}{4}a^2\omega_0^2 - \frac{K_1^2}{(\rho+K_2)^2} > 0. \tag{12}$$

This is the squared rate of amplitude growth. The fastest growing mode $q_{\rm f}$ is the one which maximizes $\Gamma(q)$. The allowed detuning for each 'oscillator' q, i.e., the actuation frequency range providing resonance, is obtained from the inequality $\epsilon^2(q) < \Gamma^2(q)$. To simplify the discussion, we will assume perfect tuning,

$$\epsilon = 0, \qquad \omega_1 = 2\omega_0(q). \tag{13}$$

Thus, by "unstable band" we will refer simply to the set of tuned 'oscillators' (i.e., range of q) for which $\Gamma^2(q) > 0$.

4 Results

4.1 Elastic substrate

The kernel $K(x-x', t-t')$ gives the nonlocal time-dependent force density, acting at a point on the medium's surface at a certain time, in response to a normal surface displacement occurring elsewhere at a different time. For a semi-infinite elastic medium, its Fourier transform was calculated by Lamb [30],

$$\tilde{K}(q,\omega) = \frac{4G^2|q|^3}{\rho_{\rm m}\omega^2}\left[\left(1 - \frac{\rho_{\rm m}\omega^2}{Gq^2}\right)^{1/2} - \left(1 - \frac{\rho_{\rm m}\omega^2}{2Gq^2}\right)^2\right], \tag{14}$$

where G is the medium's shear modulus, and we assume for simplicity an incompressible medium. In both limits of low and high frequency, this expression reduces to the form given by Eq. (4), with $K_1 = 0$, and

$$\omega \ll (G/\rho_{\rm m})^{1/2}|q| : \quad K_0 = 2G|q|, \quad K_2 = \frac{3\rho_{\rm m}}{2|q|}, \tag{15a}$$

$$\omega \gg (G/\rho_{\rm m})^{1/2}|q| : \quad K_0 = 4G|q|, \; K_2 = \frac{\rho_{\rm m}}{|q|}. \tag{15b}$$

Thus, the limits of high and low frequency differ by just numerical prefactors.[2,3]

The two regimes defined in Eq. (15) can be rewritten as $\omega/\omega_{\rm m} \ll \lambda_{\rm c} q$ and $\omega/\omega_{\rm m} \gg \lambda_{\rm c} q$. In the present problem, however, the frequency (of actuation) and the (excited) wavenumber are inter-related. As we shall see shortly, for $\omega \ll \omega_{\rm m}$ we get $\lambda_{\rm c} q \sim \omega/\omega_{\rm m}$, and for $\omega \gg \omega_{\rm m}$, $\lambda_{\rm c} q \ll \omega/\omega_{\rm m}$; namely, the first limit never strictly holds. Hence, we will assume the second limit and use Eq. (15b). Since the two behaviors are essentially the same up to constant prefactors, this choice should not have a qualitative effect. We return to this point in Sect. 5.

To make the expressions concise, we hereafter use B as the unit of energy, $(B/\hat{G})^{1/3} \sim \lambda_{\rm c}$ as the unit of length, and $(\rho_{\rm m}/\hat{G})^{1/2}(B/\hat{G})^{1/3} \sim \omega_{\rm m}^{-1}$ as the unit of time. We choose to multiply G by a numerical prefactor, $\hat{G} = 2G$, such that the static wrinkle wavenumber will turn out equal to 1. The rescaling allows us to set $B = \hat{G} = \rho_{\rm m} = 1$. The 2D pressure is then measured in units of $B^{1/3}\hat{G}^{2/3}$. (In Sect. 5.1 we will rewrite the most relevant expressions in dimensional form.)

Substituting Eq. (15b) in Eqs. (10) and (12) gives ω_0 and Γ for the case of an elastic substrate, including the inertia of both substrate and sheet. However, based on the estimates in Sect. 2, and to simplify the results, we hereafter neglect the sheet's inertia. Setting $\rho \to 0$ in these equations gives

$$\omega_0^2(q) = q^2(q^3 - P_0 q + 2), \tag{16}$$

$$\Gamma^2(q) = \frac{P_1^2 q^2}{4(q^3 - P_0 q + 2)}. \tag{17}$$

Static wrinkling appears when $\omega_0 = 0$. This occurs at the critical pressure and wavenumber

$$P_{0\rm c} = 3, \qquad q_{\rm c} = 1. \tag{18}$$

For $P_0 < P_{0\rm c}$, we have $\omega_0^2(q) > 0$ and $\Gamma^2(q) > 0$ for all q regardless of P_1. Thus, all wrinkling modes q are oscillatory and will resonate if excited by $\omega_1 = 2\omega_0(q)$. The resonance does not require the actuation amplitude to exceed a finite threshold, $P_{1\rm c} = 0$; the growth rate simply increases linearly with P_1 (Eq. (17)). This is due to the absence of damping ($K_1 = 0$).

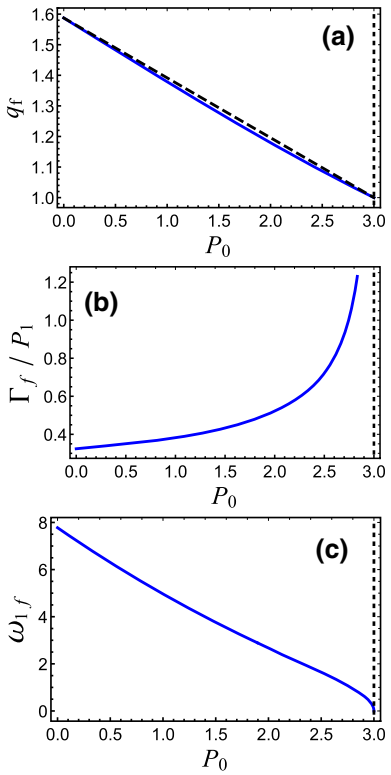

Fig. 2 Properties of the fastest-growing mode as a function of static pressure for an elastic substrate. **a** Wavenumber (solid line). The dashed line shows a linear interpolation between the analytically known wavenumbers $q_{\rm f}(0) = 2^{2/3}$ and $q_{\rm f}(P_{0\rm c}) = 1$. **b** Growth rate, diverging at $P_{0\rm c}$. For an elastic substrate, it is proportional to the actuation pressure P_1. **c** Actuation frequency required to excite the fastest-growing mode, vanishing at $P_{0\rm c}$. All parameters are normalized (see text)

Maximizing Eq. (17) gives the fastest-growing mode $q_{\rm f}(P_0)$ and its rate of amplitude growth $\Gamma_{\rm f}(P_0, P_1)$. These functions are shown in Fig. 2a, b. Also shown, in panel (c), is the actuation frequency $\omega_{1\rm f}(P_0)$ required to excite the fastest-growing mode, as obtained from Eqs. (13) and (16). For $P_0 = 0$ (uncompressed sheet), we have $q_{\rm f} = 2^{2/3} \simeq 1.59$, $\Gamma_{\rm f}/P_1 = 2^{-5/6}3^{-1/2} \simeq 0.324$, and $\omega_{1\rm f} = 2^{13/6}3^{1/2} \simeq 7.78$. Thus, the fastest-growing wavelength is smaller than that of the static wrinkles. As the static pressure is increased, $q_{\rm f}$ decreases (wavelength increases), $\Gamma_{\rm f}/P_1$ increases, and $\omega_{1\rm f}$ decreases, until, at $P_0 = P_{0\rm c} = 3$, the wavelength converges to the static one, $\omega_{1\rm f}$ vanishes, and $\Gamma_{\rm f}$ diverges.

The fastest-growing mode, however, is not the selected resonant mode. The natural control parameters in experiment are the static pressure, the actuation frequency, and the actuation amplitude. Given P_0, the choice of ω_1 selects a dynamic wrinkle wavenum-

[2] Note that at intermediate frequencies this kernel describes a more complex response, including imaginary (yet still time-reversible) terms.

[3] In the static limit ($\omega = 0$), one recovers the result derived from the Boussinesq problem [31], $\tilde{K}(q, 0) = 2G|q|$.

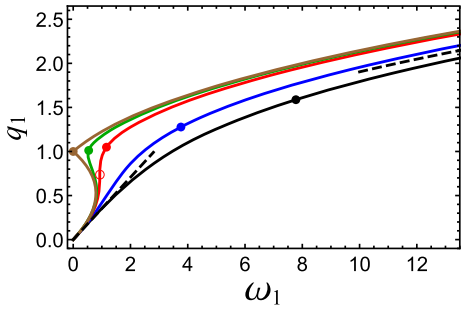

Fig. 3 Wrinkle wavenumber as a function of actuation frequency for an elastic substrate. Different curves correspond to different values of static pressure P_0 (from right to left): 0, 1.5, $P_0^* = 20^{1/3}$, 2.93, and $P_{0c} = 3$. Solid circles indicate the fastest-growing mode for the corresponding pressure. Dashed lines show the asymptotes given in Eq. (19). For $P_0 > P_0^*$, there are three solutions for q_1, the largest of which growing the fastest, implying a discontinuous jump in the observed dominant wavenumber as ω_1 is ramped up. The empty circle marks the bifurcation point. All parameters are normalized (see text)

ber, $q_1(\omega_1, P_0)$, according to Eqs. (13) and (16). This wavenumber is not equal to q_f in general and is independent of P_1. Figure 3 shows the selected wavenumber as a function of ω_1 for several values of P_0 between 0 and P_{0c}. The figure shows also the asymptotes of q_1 for small and large ω_1, which are both independent of P_0,

$$q_1(\omega_1, P_0) \simeq \begin{cases} 2^{-3/2}\,\omega_1, & \omega_1 \ll 1 \\ (\omega_1/2)^{2/5}, & \omega_1 \gg 1. \end{cases} \tag{19}$$

The corresponding asymptotes for the rate of amplitude growth are

$$\Gamma(\omega_1, P_0, P_1) \simeq \begin{cases} (P_1/8)\,\omega_1, & \omega_1 \ll 1 \\ P_1(16\,\omega_1)^{-1/5}, & \omega_1 \gg 1. \end{cases} \tag{20}$$

The asymptotes in Eq. (19) confirm our earlier statement, that q_1 is never much smaller than ω_1, in dimensionless terms. Switching for a moment back to dimensional parameters, the two asymptotes become $q_1 \sim (\rho_m/G)^{1/2}\omega_1$ and $q_1 \sim (\rho_m/B)^{1/5}\omega_1^{2/5}$, revealing the different physical mechanisms in the two limits. At low frequencies, the restoring mechanism is the substrate's elasticity, whereas at high frequencies it is the sheet's bending rigidity. This crossover was anticipated in Sect. 2. Less expected is the finding that the change between the two behaviors may be discontinuous, as we shall see now.

At $P_0 = P_0^* = (20)^{1/3} \simeq 2.71$ and $\omega_1 = \omega_1^* = 2(2/5)^{5/6} \simeq 0.932$, the selected wavenumber, which is at this point $q_1^* = (2/5)^{1/3} \simeq 0.737$, bifurcates into three (Fig. 3). The bifurcation entails anomalous dynamics. At the bifurcation point, we have $\mathrm{d}\omega_0/\mathrm{d}q = 0$, implying that an excitation with P_0^* and ω_1^* at one edge of the sheet will not propagate through the sheet. For $P_0 > P_0^*$ and $\omega_1 < \omega_1^*$, we find from Eq. (17) that the

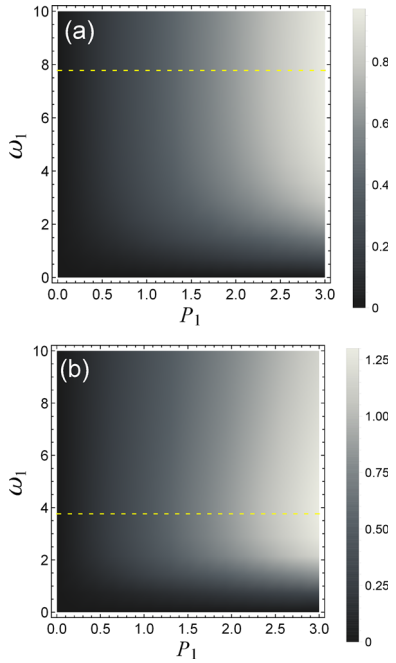

Fig. 4 Density plots of wrinkle growth rate as a function of excitation amplitude and frequency for an elastic substrate. The static pressure values are **a** $P_0 = 0$ and **b** $P_0 = P_{0c}/2 = 3/2$. The dashed lines show ω_{1f}, the excitation frequency that produces the fastest-growing mode (which for an elastic substrate is independent of P_1). All parameters are normalized (see text).

largest of the three solutions for $q_1(\omega_1, P_0)$ grows the fastest. Thus, for $P_0 > P_0^*$, as the excitation frequency ω_1 is gradually increased from 0, the selected wrinkle wavenumber will undergo a discontinuous jump. For increasingly larger static pressure P_0, the jump occurs at lower and lower frequencies (see Fig. 3), until, at $P_0 = P_{0c}$, the system selects $q_1 = q_c$ at zero frequency, as it should. This is how the static-wrinkling limit is reproduced from the dynamic one. Note that this entire behavior is independent of P_1; hence, the discontinuous transition is present also for arbitrarily weak actuation.

Figure 4 presents 2D maps of the growth rate Γ as a function of P_1 and ω_1 for $P_0 = 0$ and $P_0 = P_{0c}/2$.

4.2 Viscoelastic substrate

For a viscoelastic medium, the response is generalized by replacing G with a frequency-dependent complex shear modulus $\tilde{G}(\omega)$. (Recall that we have been assuming an incompressible medium.) Applying the single-relaxation approximation of Eq. (4), we generalize Eq. (15b) above to

$$K_0 = 4G|q|, \quad K_1 = 4\eta|q|, \quad K_2 = \rho_m/|q|, \tag{21}$$

where $G = \mathrm{Re}(\tilde{G})$ and $\eta = \mathrm{Im}(\tilde{G})/\omega$ are the substrate's 'store' modulus and viscosity, respectively ($\omega\eta$ is the 'loss' modulus). We use the same units of energy, length,

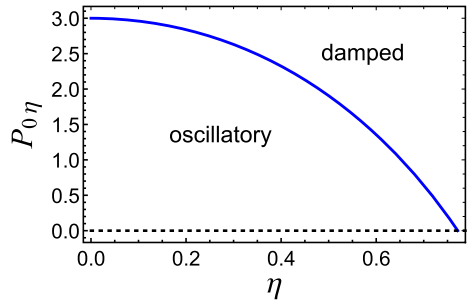

Fig. 5 Oscillatory and damped modes for a viscoelastic substrate. At static pressures smaller than $P_{0\eta}(\eta)$ (solid curve), all modes are oscillatory; at larger pressures, increasingly more modes are damped. For $\eta = 0$ (elastic substrate), all modes are oscillatory for any $P_0 < P_{0c} = 3$. All parameters are normalized (see text)

and time as in Sect. 4.1, making B, $\hat{G} = 2G$, and ρ_m all equal to unity. The viscosity η is measured then in units of $\rho_m^{1/2}\hat{G}^{1/6}B^{1/3}$.

Substituting Eq. (21) in Eqs. (10) and (12) while neglecting ρ, we obtain

$$\omega_0^2(q) = q^2(q^3 - 4\eta^2 q^2 - P_0 q + 2), \tag{22}$$

$$\Gamma^2(q) = \left[\frac{P_1^2}{4(q^3 - 4\eta^2 q^2 - P_0 q + 2)} - 16\eta^2 q^2\right] q^2. \tag{23}$$

The viscous component leads to several essential changes compared to the elastic case. First, for a given η, P_0 has to be smaller than some $P_{0\eta}(\eta) < P_{0c}$ to have all modes oscillatory ($\omega_0^2 > 0$). The limiting function $P_{0\eta}(\eta)$ is shown in Fig. 5. As one approaches the static wrinkling transition, increasingly more modes become damped. For $\eta > 2^{-7/6}3^{1/2} \simeq 0.772$, $P_{0\eta} < 0$, i.e., there are damped modes for any static pressure (unless we 'strengthen the springs' by stretching the sheet with $P_0 < 0$).

As in the elastic case, fixing $\omega_1 = 2\omega_0$ selects a mode, $q_1(\omega_1, P_0, \eta)$, which does not depend on P_1 (see Eq. (22)). Unlike the elastic case, the fastest-growing mode $q_f(P_0, P_1, \eta)$, obtained by maximizing Γ of Eq. (23), does depend on P_1. Hence, the fastest-growing mode does not belong in general to the set of selected wavenumbers; one should tune P_1 together with ω_1 to get $q_1 = q_f$ (see Fig. 8 below). Figure 6a shows the selected wavenumber as a function of ω_1 for several values of P_0 between 0 and P_{0c}. The asymptotes for small and large ω_1 remain as in Eq. (19). Also here, the solutions bifurcate above a certain static pressure P_0^*, implying a discontinuous jump in the dominant wrinkle wavenumber as ω_1 is increased. The bifurcation point depends now on η. (See the Supplementary Material [27] for the functional dependence.) Figure 6b shows the decrease of P_0^* with η. For sufficiently high viscosity, $\eta > 3^{1/2}5^{1/3}/4 \simeq 0.740$, the change of wavenumber with frequency is discontinuous for any P_0. Finally, for $P_0 > P_{0\eta} > P_0^*$ a band of modes becomes damped (with

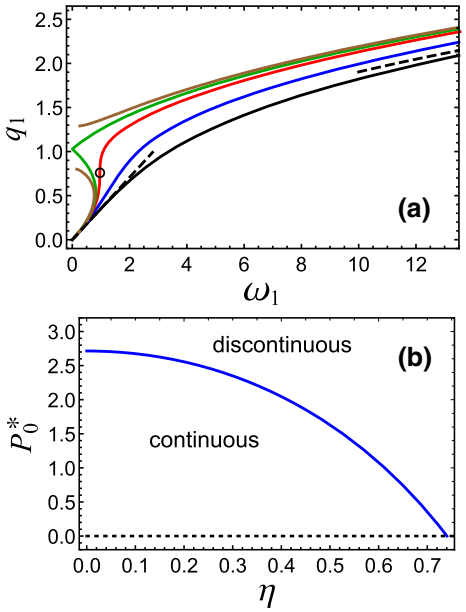

Fig. 6 Change of wrinkle wavenumber with actuation frequency for a viscoelastic substrate. **a** Wavenumber as a function of frequency for a given viscosity, $\eta = 0.2$. Different curves correspond to different values of static pressure P_0 (from right to left): 0, $P_{0c}/2 = 3/2$, $P_0^* = 2.55$, $P_{0\eta} = 2.84$, and $P_{0c} = 3$. Dashed lines show the asymptotes given in Eq. (19). For $P_0 > P_0^*$, there are three solutions for q_1, the largest of the three growing the fastest, implying a discontinuous jump in the observed dominant wavenumber as ω_1 is ramped up. The empty circle marks the bifurcation point. For $P_0 > P_{0\eta}$, a band of modes are damped (leftmost, brown curve). **b** Decrease in the bifurcation pressure with viscosity. All parameters are normalized (see text)

imaginary ω_0) as manifested by the leftmost curve in Fig. 6a.

Another important change brought about by viscosity is that the oscillatory modes do not resonate for every value of P_1 and ω_1. The expression for the squared growth rate in Eq. (23) has the asymptotes $(P_1^2/8)q^2$ and $-16\eta^2 q^4$, respectively, at small and large q. Thus, for any finite P_1 there are small-q resonant modes, but the unstable band has a cutoff at some $q_{max}(P_0, P_1, \eta)$. The reason why resonance should require small wavenumber lies in the dependence of inertia on q (cf. K_2 in Eq. (21)). The larger the wavelength, the thicker the layer of substrate which moves with the sheet, and the larger its inertia. Figure 7 shows the dependence of the cutoff q_{max}, along with the fastest-growing mode q_f, on P_1 for an uncompressed sheet ($P_0 = 0$) and a given viscosity. Equation (23) can be rewritten as

$$\Gamma^2 = \left(\frac{P_1^2}{\omega_1^2} - 16\eta^2\right) q^4. \tag{24}$$

Hence, resonance requires crossing a threshold of actuation amplitude, which is linear in the actuation frequency,

$$P_1 > P_{1c} = 4\eta\omega_1. \tag{25}$$

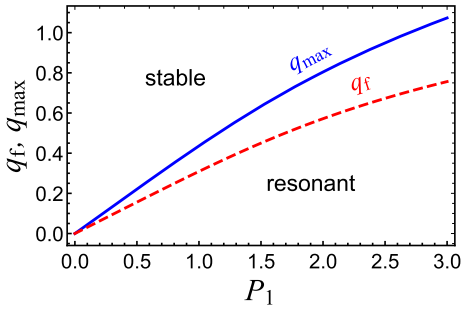

Fig. 7 Unstable (resonant) band as a function of actuation amplitude for an uncompressed sheet ($P_0 = 0$) on a viscoelastic substrate. The viscosity is $\eta = 0.2$. For q larger than the cutoff q_{max} (solid line), the modes are stable (of finite amplitude). Also shown is the fastest-growing mode q_f (dashed line). All parameters are normalized (see text)

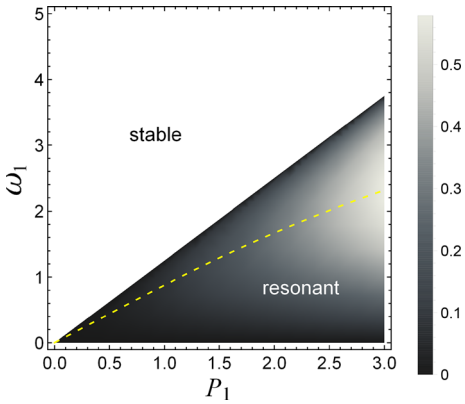

Fig. 8 Density plot of wrinkle growth rate as a function of actuation amplitude and frequency for an uncompressed sheet ($P_0 = 0$) on a viscoelastic substrate. The viscosity is $\eta = 0.2$. The resonant band is bounded by a minimum amplitude proportional to ω_1. The dashed line shows the excitation frequency that produces the fastest-growing mode for each actuation amplitude. All parameters are normalized (see text)

This is a consequence of the viscous damping. The smaller the frequency, the weaker the actuation needed to overcome the damping. The reason, once again, is that a larger mass of substrate is involved in the motion for small wavenumber (low frequency).

Figure 8 shows a 2D map of the growth rate Γ as a function of the excitation parameters P_1 and ω_1 for an uncompressed sheet ($P_0 = 0$). Unlike the elastic-substrate case (Fig. 4), here the resonant region is bounded.

5 Discussion

5.1 Summary of experimental predictions

Let us summarize the results which seem most relevant experimentally and give them in dimensional form. As in the analysis above, we assume that the inertia is governed by the substrate. A similar discussion for the case of sheet-dominated inertia is given in the Supplementary Material [27].

In the case of an elastic substrate, one can first compress the sheet until static wrinkling occurs. The measured critical pressure and static wrinkle wavenumber are related to the bending modulus of the sheet and the elastic modulus of the substrate as

$$P_{0c} = 3B^{1/3}G^{2/3}, \quad q_c = (G/B)^{1/3}, \tag{26}$$

with known corrections for finite compressibility [28]. This allows a measurement of B and G.

For a finite $P_0 < P_{0c}$, and ramping up the actuation frequency ω_1 from zero, dynamic wrinkles should form for any actuation amplitude. At low frequency ($\omega_1 \ll \omega_m \sim (G/\rho_m)^{1/2}/\lambda_c$), the wrinkle wavenumber q_1 increases linearly with ω_1,

$$q_1 \simeq (1/4)(\rho_m/G)^{1/2}\,\omega_1, \tag{27a}$$

which is essentially the relation for Rayleigh surface waves [29]. At high frequencies ($\omega_1 \gg \omega_m$), the wavenumber increases as $\omega_1^{2/5}$,

$$q_1 \simeq 0.758(\rho_m/B)^{1/5}\,\omega_1^{2/5}. \tag{27b}$$

Concerning the dependence on sheet thickness, at low frequencies the wrinkle wavenumber is independent of h, and at high frequencies it decreases with h as $\sim h^{-3/5}$. These very different dependencies are related to the different restoring mechanisms in the two regimes. At low frequency, the substrate's elasticity dominates, and the resulting Rayleigh waves are independent of the sheet. At high frequency, the dominant force comes from the sheet's bending rigidity, which depends on thickness. The two dependencies are to be compared with that of the static wrinkles, where $q_c \sim h^{-1}$; see Eq. (26).

Depending on the value of P_0, two distinct behaviors are expected as ω_1 is increased. At small pressures, $P_0 < P_0^*$, the selected wrinkle wavelength decreases continuously with ω_1. For larger pressures, $P_0^* < P_0 < P_{0c}$, a discontinuous drop in the dominant wavelength is expected as a function of ω_1. The transition occurs at

$$P_0^* = 0.905P_{0c}. \tag{28}$$

The transition in the wrinkle wavelength is a particularly distinctive prediction. We discuss its validity further in Sect. 5.3 below.

The behavior in the case of a viscoelastic substrate is qualitatively different. Thus, it might be used to obtain information on the viscoelastic properties of the supporting medium. The present theory is restricted, however, to the simple case where the viscoelastic response is described sufficiently well by a single relaxation time, $\tau = \eta/G$, i.e., the complex modulus is given by $\tilde{G} =$

$G + i\omega\eta$; cf. Sects. 3.2 and 4.2. The static measurement of P_{0c} and q_c are as in the elastic case above.

To see dynamic wrinkles on a viscoelastic substrate, one needs an excitation with pressure amplitude that exceeds a threshold P_{1c}. The threshold depends linearly on the excitation frequency,

$$P_{1c} = 3.17\eta(B/G)^{1/3}\,\omega_1 = 3.17\eta\lambda_c\,\omega_1. \qquad (29)$$

where λ_c is the static wrinkle wavelength. Thus, the threshold of resonance may be used as a probe of the viscous component η. As in the elastic case, at low and high excitation frequencies the asymptotic dependence of the dynamic wrinkle wavenumber q_1 on ω_1 is given in Eqs. (27). The remark concerning the dependence on sheet thickness in the elastic case holds here as well.

In the viscoelastic case, too, the value of P_0 separates the behaviors when ramping up ω_1 into two cases: a continuous decrease in wavelength for low pressure and a discontinuous one at high pressure. The transition pressure P_0^* decreases with viscosity (see Fig. 6b and the Supplementary Material [27]), providing another probe of η.

To get a feeling for the relevant scales, we consider a specific system, motivated by the experimental system of Ref. [4]. It is made of a 1-mm-thick stiffer elastomeric sheet ($E_s \sim 10^6$ Pa), supported on a softer elastomeric medium ($E_m \sim 10^4$ Pa). These properties fit also a layer of skin covering a muscle tissue. The sheet's bending modulus is $B \sim 10^{-4}$ J. The resulting static wrinkle wavenumber (Eq. (26)) is $q_c \sim 1$ mm^{-1}. (This is at the edge of the theory's validity, which requires $qh \ll 1$; thus, the following should be regarded only as qualitative orders of magnitude.) To excite dynamic wrinkles of a similar wavenumber, we need, according to Eq. (27), an excitation frequency of order $\omega_1 \sim 10^4$ s^{-1}. (We have taken $\rho_m \sim 10^3$ kg/m^3.) This is close to the relevant lower frequency bound obtained in Sect. 1. As already noted there, such frequencies are probably too high to be produced naturally but readily attainable in experiments.

To observe the viscous effects described in Sect. 4.2, we need a normalized η of order 1. In dimensional terms, it implies, for the example above, $\eta \gtrsim$ 1–10 Pa s (i.e., 10^3–10^4 times the viscosity of water). This is in line with the estimate in Sect. 2.

5.2 Comparison with other dynamic wrinkling scenarios

As mentioned in Sect. 1, several works have addressed the formation of dynamic wrinkles in thin sheets upon time-varying external forcing, whose source may be, for example, the impact of a rigid object, or an abrupt change of pressure or confinement [18–24]. The main feature that sets the system addressed here apart is the periodic, single-frequency external forcing. Within our linear theory, it implies the selection of a single, constant wrinkle wavelength. For the non-periodic forcing in the other scenarios, a time-increasing (coarsening) wavelength has been observed (e.g., Ref. [20]). Unlike the periodically excited system, the other systems eventually approach equilibrium whereby the dynamic wavelength must tend toward its static value.

In addition, parametric resonance has a different mode-selection mechanism. The mode q_1 is selected to match the actuation frequency (such that $2\omega_0(q_1) = \omega_1$). Thus, it is not equal to the fastest-growing mode q_f, which is the selected mode in the other scenarios. One consequence concerns the dependence of the selected mode on inertia. In the absence of damping, the mode which maximizes the growth rate in our system is independent of ρ_m. (See Eqs. (10) and (12) in which, for $K_1 = 0$, the mass density enters only in a prefactor.) Similarly, the selected pattern in other dynamic-buckling systems was found to be independent of inertia (e.g., Ref. [24]). In the resonant system, the selected mode q_1 does not maximize the growth rate and thus depends on ρ_m.

Nevertheless, there is a qualitative relation with the time dependence of the selected mode in a supported sheet under impact [20]. In Ref. [20], the selected wavelength was found to increase with time according to $\lambda(t) \sim (B/\rho_m)^{1/5}\,t^{2/5}$. This scaling is in line with our $q_1(\omega_1)$ relation in the high-frequency limit, Eq. (27b). It arises in both cases from the interplay of sheet bending and substrate inertia (see Sect. 2). Consistently with this limit, the wavelength values measured in the impact experiments were much smaller than λ_c. With a compressed sheet on a (visco)elastic substrate, the impact behavior at longer times (corresponding to our low-frequency-large-wavelength limit, Eq. (27a)) might reveal an instability or a two-wave pattern similar to the one predicted above for $q_1(\omega_1)$.

5.3 Model extensions

We have assumed above that the inertia is governed by the substrate. As estimated in Sect. 1, this is valid when the wavelength is much larger than the sheet thickness. When the two are not scale-separated, the sheet's inertia may be important. (In fact, this may be the case in the numerical example given above.) The physical difference between the two limits is the fact that the effective 2D mass responsible for inertia in the substrate case depends on wavelength (cf. K_2 of Eq. (15)), whereas for the sheet it is a constant. The combination of inertial effects from both substrate and sheet can be treated within our theory. One should return to the equations of motion, Sect. 3.2 and consider the full inertial terms with $\rho_s h + K_2(q)$ instead of just K_2. The algebra is more cumbersome but can be treated numerically.

The opposite limit, of sheet-dominated inertia, is presented in the Supplementary Material [27]. Although this limit is of less practical relevance, it is instructive to see the qualitative changes brought about by the sheet's mass. These are as follows. (a) The fastest growing wavelength for an uncompressed sheet ($P_0 = 0$) is arbitrarily small (whereas with substrate inertia it is $\sim \lambda_c$; see Fig. 2). Thus, a finite static pressure is

required to get finite-size dynamic wrinkles. (b) The selected wavenumber scales differently with actuation frequency, as ω_1^2 and $\omega_1^{1/2}$ at low and high frequency, respectively. (Compare to Eq. (19)) (c) As a result of (b), the dependence of wrinkle wavenumber on sheet thickness is different — increasing as h and decreasing as $h^{-1/2}$ for large and small ω_1, respectively (compared to h^0 and $h^{-3/5}$ with substrate inertia). Overall, however, the qualitative behaviors are quite similar. In particular, the phenomenon of continuous vs. discontinuous change of selected wavelength with frequency exists in both limits.

We have used the large-frequency asymptotic form of the substrate's kernel, Eq. (15b). The small-frequency asymptote is the same up to numerical prefactors (see Eq. (15)) and will lead to the same results. A more complete theory should consider the full kernel, Eq. (14). This would require a more complicated numerical analysis. One might be worried that our central prediction, concerning the continuous vs. discontinuous behavior of q_1 as a function of ω_1, is an artifact of the asymptotic kernel, as the phenomenon occurs at $q_1\lambda_c \sim 1$ (see Figs. 3 and 6). This is most probably not the case. The transition is a result of the function $\omega_0^2(P_0, q)$ becoming non-convex at sufficiently high pressure. It is a generic property required to obtain the static wrinkling transition, $\omega_0^2(P_{0c}, q_c) = 0$, at a finite wavenumber q_c. Indeed, the case of sheet-dominated inertia [27], where the much simpler kernel of a static elastic substrate is fully treated, exhibits the same behavior.

The theory presented here is linear. As a result, it provides the properties of the instability but not the ultimate form of the sheet's dynamic deformation. Whether the deformation saturates to periodic wrinkles of finite height, develops multi-wavelength wrinkles [32], or localizes into deeper features (folds) [20,33], should be checked in a future nonlinear theory or simulation.

We have assumed a semi-infinite substrate. Over length scales comparable and larger than the substrate thickness, the results will be modified. In the opposite limit, of a thin substrate compared to the wrinkle wavelength, the effect of the medium will turn into that of a Winkler foundation [34], i.e., strongly localized ($\tilde{K}$ independent of q).

Another simplification employed here is the assumption of a single relaxation time for the viscoelastic medium. Actual viscoelastic media, particularly biological ones, have a much richer frequency dependence, which will affect the response to the parametric excitation. Conversely, parametric resonance may be used to tap into the medium's rich temporal response based on an extended theory.

Besides relaxation times, complex media have also characteristic lengths which affect their response [35,36]. The present theory describes a way to sample various length scales (wavenumbers) by sweeping the parametric-excitation frequency. Recently, we have derived the solution to the Boussinesq problem for a viscoelastic structured medium, accounting for its intrinsic correlation length [37]. Similar to the derivations in Sects. 4.1 and 4.2, these results (once extended to include inertia) may be used to address the parametric excitation of a sheet supported on such a structured medium.

Supplementary information The online version contains supplementary material available at https://doi.org/10.1140/epje/s10189-021-00085-y.

Acknowledgements Helpful discussions with Benny Davidovitch, Oz Oshri, and Luka Pocivavsek are gratefully acknowledged.

Author contribution statement

The author performed the research and writing of the manuscript.

References

1. E. Cerda, L. Mahadevan, Geometry and physics of wrinkling. Phys. Rev. Lett. **90**, 074302 (2003)
2. J. Genzer, J. Groenewold, Soft matter with hard skin: From skin wrinkles to templating and material characterization. Soft Matter **2**, 310–323 (2006)
3. B. Davidovitch, R.D. Schroll, D. Vella, M. Adda-Bedia, E. Cerda, Prototypical model for tensional wrinkling in thin sheets. Proc. Natl. Acad. Sci. USA **108**, 18227–18232 (2011)
4. L. Pocivavsek, J. Pugar, R. O'Dea, S.-H. Ye, W. Wagner, E. Tzeng, S. Velankar, E. Cerda, Topography-driven surface renewal. Nat. Phys. **14**, 948–953 (2018)
5. L. Pocivavsek, S.-H. Yea, J. Pugar, E. Tzeng, E. Cerda, S. Velankar, W.R. Wagnera, Active wrinkles to drive self-cleaning: A strategy for anti-thrombotic surfaces for vascular grafts. Biomat. **192**, 226–234 (2019)
6. N.N. Nath, L. Pocivavsek, J.A. Pugar, Y. Gao, K. Salem, N. Pitre, R. McEnaney, S. Velankar, E. Tzeng, Dynamic luminal topography: A potential strategy to prevent vascular graft thrombosis. Front. Bioeng. Biotech. **8**, 573400 (2020)
7. G. Lin, W. Sun, P. Chen, Topography-driven delamination of thin patch adhered to wrinkling surface. Int. J. Mech. Sci. **178**, 105622 (2020)
8. X. Wen, S. Sun, P. Wu, Dynamic wrinkling of a hydrogel-elastomer hybrid microtube enables blood vessel-like hydraulic pressure sensing and flow regulation. Mater. Horiz. **7**, 2150 (2020)
9. D. Vella, J. Bico, A. Boudaoud, B. Roman, P.M. Reis, The macroscopic delamination of thin films from elastic substrates. Proc. Natl. Acad. Sci. USA **106**, 10901–10906 (2009)
10. H. Mei, C.M. Landis, R. Huang, Concomitant wrinkling and buckle-delamination of elastic thin films on compliant substrates. Mech. Mater. **43**, 627–642 (2011)
11. E. Hohfeld, B. Davidovitch, Sheet on a deformable sphere: Wrinkle patterns suppress curvature-induced delamination. Phys. Rev. E **91**, 012407 (2015)

12. O. Oshri, Y. Liu, J. Aizenberg, A.C. Balazs, Delamination of a thin sheet from a soft adhesive Winkler substrate. Phys. Rev. E **97**, 062803 (2018)
13. O. Oshri, Delamination of open cylindrical shells from soft and adhesive Winkler's foundation. Phys. Rev. E **102**, 033001 (2020)
14. G.D. Bixler, B. Bhushan, Biofouling: Lessons from nature. Phil. Trans. R. Soc. A **370**, 2381–2417 (2012)
15. N. Sridhar, D.J. Srolovitz, Z. Suo, Kinetics of buckling of a compressed film on a viscous substrate. Appl. Phys. Lett. **78**, 2482–2484 (2001)
16. R. Huang, Z. Suo, Wrinkling of a compressed elastic film on a viscous layer. J. Appl. Phys. **91**, 1135–1142 (2002)
17. R. Huang, Kinetic wrinkling of an elastic film on a viscoelastic substrate. J. Mech. Phys. Solids **53**, 63–89 (2005)
18. R. Vermorel, N. Vandenberghe, E. Villermaux, Impacts on thin elastic sheets. Proc. Roy. Soc. A **465**, 823–842 (2009)
19. N. Vandenberghe, L. Duchemin, Impact on floating membranes. Phys. Rev. E **93**, 052801 (2016)
20. F. Box, D. O'Kiely, O. Kodio, M. Inizan, A.A. Castrejón-Pita, D. Vella, Dynamics of wrinkling in ultrathin elastic sheets. Proc. Natl. Acad. Soc. USA **116**, 20875–20880 (2019)
21. M.A. Ghanem, X. Liang, B. Lydon, L. Potocsnak, T. Wehr, M. Ghanem, S. Hoang, S. Cai, N. Boechler, Wrinkles riding waves in soft layered materials. Adv. Mat. Interface **6**, 1801609 (2019)
22. O. Kodio, I.M. Griffiths, D. Vella, Lubricated wrinkles: Imposed constraints affect the dynamics of wrinkle coarsening. Phys. Rev. Fluid **2**, 014202 (2017)
23. J. Chopin, M. Dasgupta, A. Kudrolli, Dynamic wrinkling and strengthening of an elastic filament in a viscous fluid. Phys. Rev. Lett. **119**, 088001 (2017)
24. F. Box, O. Kodio, D. O'Kiely, V. Cantelli, A. Goriely, D. Vella, Dynamic buckling of an elastic ring in a soap film. Phys. Rev. Lett. **124**, 198003 (2020)
25. H. Vandeparre, S. Gabriele, F. Brau, C. Gay, K.K. Parker, P. Damman, Hierarchical wrinkling patterns. Soft Matter **6**, 5751–5756 (2010)
26. L.D. Landau, E.M. Lifshitz, *Mechanics*, 2nd edn. (Pergamon Press, Oxford, 1960), sect. V.27
27. See Supplementary Material
28. J. Groenewold, Wrinkling of plates coupled with soft elastic media. Physica A **298**, 32–45 (2001)
29. L.D. Landau, E.M. Lifshitz, *Theory of Elasticity*, 3rd edn. (Butterworth-Heinemann, Oxford, 1986), sect. III.24
30. H. Lamb, On the propagation of tremors over the surface of an elastic body. Phil. Trans. A **203**, 1–42 (1904)
31. L.D. Landau, E.M. Lifshitz, *Theory of Elasticity*, 3rd edn. (Butterworth-Heinemann, Oxford, 1986), sect. I.8
32. F. Brau, H. Vandeparre, A. Sabbah, C. Poulard, A. Boudaoud, P. Damman, Multiple-length-scale elastic instability mimics parametric resonance of nonlinear oscillators. Nat. Phys. **7**, 56–60 (2011)
33. F. Brau, P. Damman, H. Diamant, T.A. Witten, Wrinkle to fold transition: influence of the substrate response. Soft Matter **9**, 8177–8186 (2013)
34. D.A. Dillard, B. Mukherjee, P. Karnal, R.C. Batra, J. Frechette, A review of Winkler's foundation and its profound influence on adhesion and soft matter applications. Soft Matter **14**, 3669–3683 (2018)
35. A. Sonn-Segev, A. Bernheim-Groswasser, H. Diamant, Y. Roichman, Viscoelastic response of a complex fluid at intermediate distances. Phys. Rev. Lett. **112**, 088301 (2014)
36. A.Y. Grosberg, J.-F. Joanny, W. Srinin, Y. Rabin, Scale-dependent viscosity in polymer fluids. J. Phys. Chem. B **120**, 6383–6390 (2016)
37. C. Bar-Haim, H. Diamant, Surface response of a polymer network: Semi-infinite network. Langmuir **36**, 247–255 (2020)